Supplementary Information

Recyclable, Ultralow-Hysteresis, Multifunctional Wearable Sensors Based on Water-Permeable, Stretchable, and Conductive Cellulose/PEDOT:PSS Hybrid Films

Anky Fitrian Wibowo, [a] Saravanan Nagappan, [b] Siti Aisyah Nurmaulia Entifar, [a] Jung Ha Kim, [a] Yulia Shara Sembiring, [a] Joo Won Han, [b] Junghwan Oh, [c] Guohua Xie, [d] Jonghee Lee, [e] Jincheol Kim, [f] Dong Chan Lim, [g] Myoung-Woon Moon, [h] Min-Seok Kim, [h] Soyeon Kim, [*g] and Yong Hyun Kim [*a,i]

[a]*Department of Smart Green Technology Engineering, Pukyong National University, Busan 48513, Republic of Korea*

[b]*Industry-University Cooperation Foundation, Pukyong National University, Busan 48513, Republic of Korea*

[c]*Department of Biomedical Engineering, Pukyong National University, Busan 48513, Republic of Korea*

[d]*Institute of Flexible Electronics (Future Technologies), Xiamen University, Xiamen, China*

[e]*Department of Creative Convergence Engineering, Hanbat National University, Daejon 34158, Republic of Korea*

[f]*School of Engineering, Sustainable Energy Research Centre, Macquarie University, Sydney, New South Wales 2109, Australia*

[g]*Surface Technology Division, Korea Institute of Materials Science (KIMS), Changwon 51508, Republic of Korea*

[h]*Advanced Materials Research Division, Extreme Materials Research Center, Korea Institute of Science and Technology, Seoul 02792, Republic of Korea*

[i]*School of Electrical Engineering, Pukyong National University, Busan 48513, Republic of Korea*

*Corresponding author. E-mail: yhkim113@pknu.ac.kr (Yong Hyun Kim) E-mail: kimso1965@kims.re.kr (Soyeon Kim)

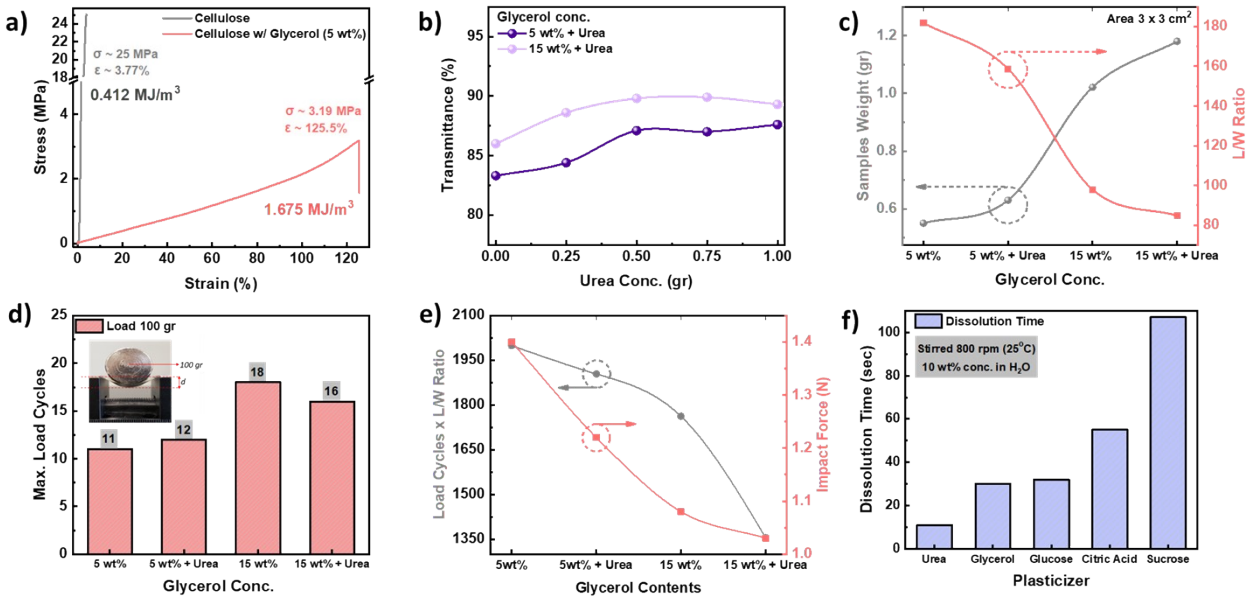

Figure S1. (a) Tensile stress-strain profiles of HEC film and HEC film with 5 wt.% glycerol as a plasticizer. (b) Transmittance spectra of HEC films as a function of glycerol and urea concentrations. (c-e) Mechanical characteristics of HEC films incorporated with glycerol and urea. (f) Dissolution kinetics of different plasticizers in deionized water.

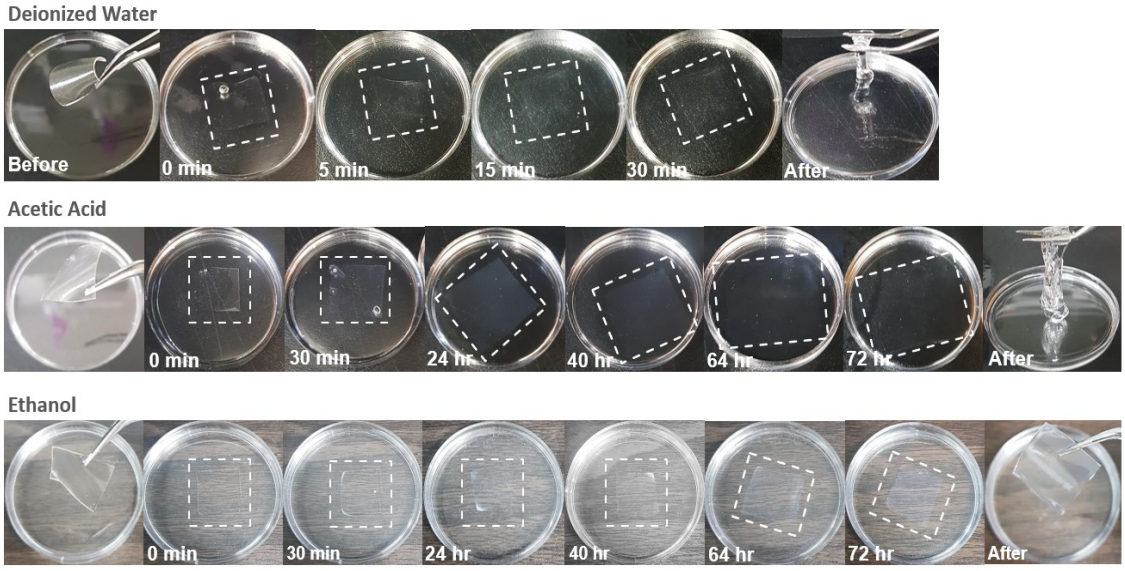

Figure S2. Degradation behavior of HEC substrates immersed in various solvents, including deionized water, acetic acid, and ethanol. Rapid dissolution of the HEC substrate occurred within 30 minutes in deionized water, whereas no dissolution was observed after 3 days in ethanol.

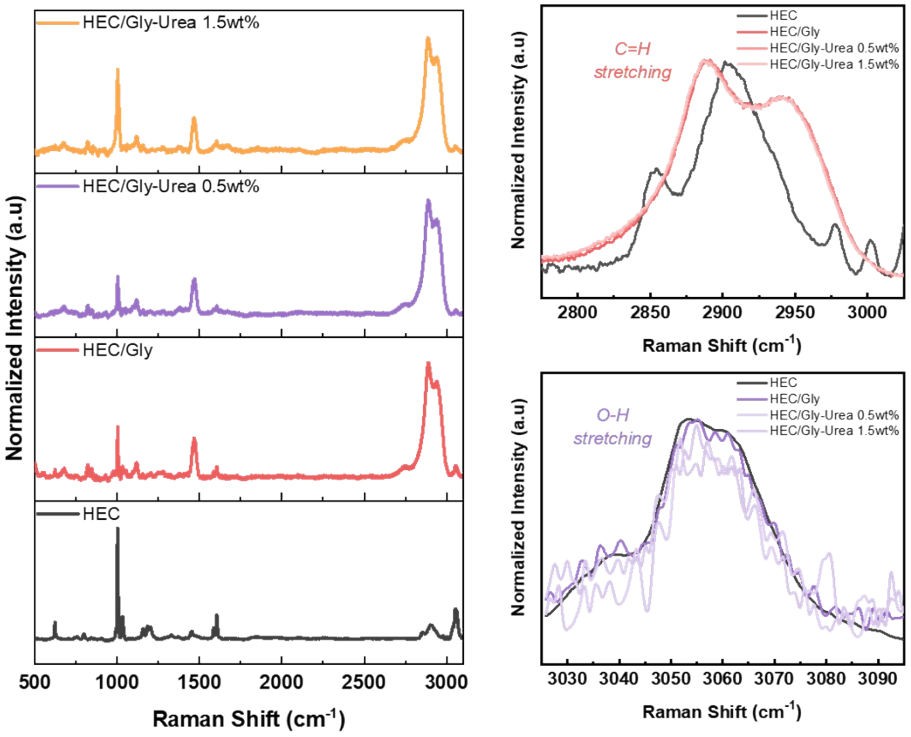

Figure S3. Raman spectroscopy analysis of pure HEC, glycerol-treated HEC, and urea/glycerol-treated HEC across the entire range of Raman shift and specifically focusing on the 2800-3100 cm^{-1} region

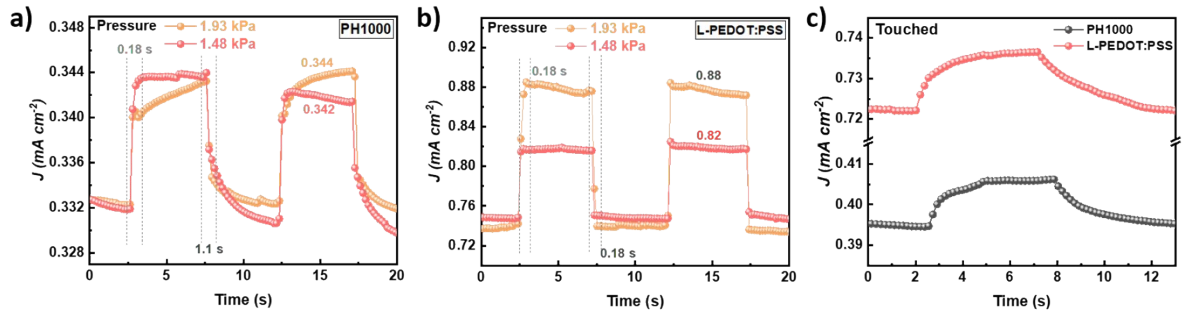

$$J = \frac{Current}{Crossection\ Area} = \frac{I\ (mA)}{A\ (cm^2)}$$

Figure S4. Variation in current density of HEC/PEDOT:PSS films under different loading conditions, including (a, b) object loading at pressures of 1.93 kPa and 1.48 kPa, and (c) finger contact.

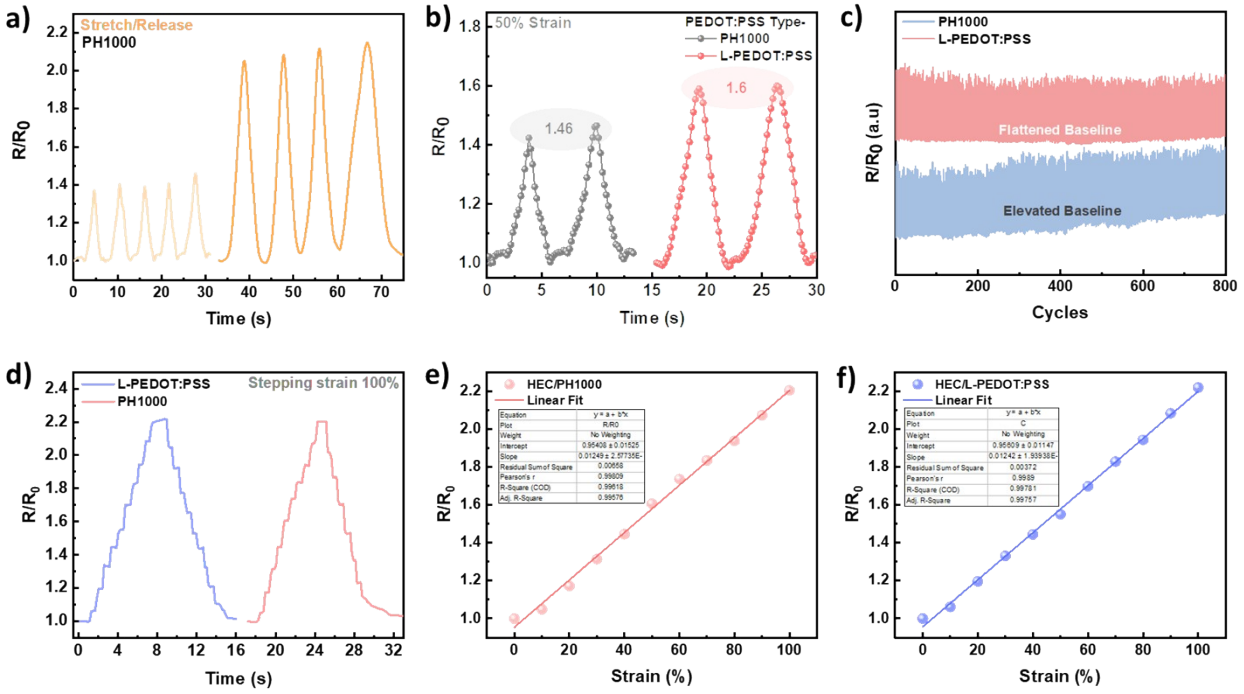

Figure S5. (a) Relative resistance changes of HEC/PH1000 composite film under cyclic stretch–release tests (50 % and 100 % strains). (b) Relative resistance (R/R_0) comparison during 50% strain for L-PEDOT:PSS and PH1000. (c) Comparative analysis of long-range (800) stretch-release cycles for L-PEDOT:PSS and PH1000. (d) Comparison of relative resistance during 100% staircase strain. (e, f) Evaluation of linearity in HEC/PEDOT:PSS composite films.

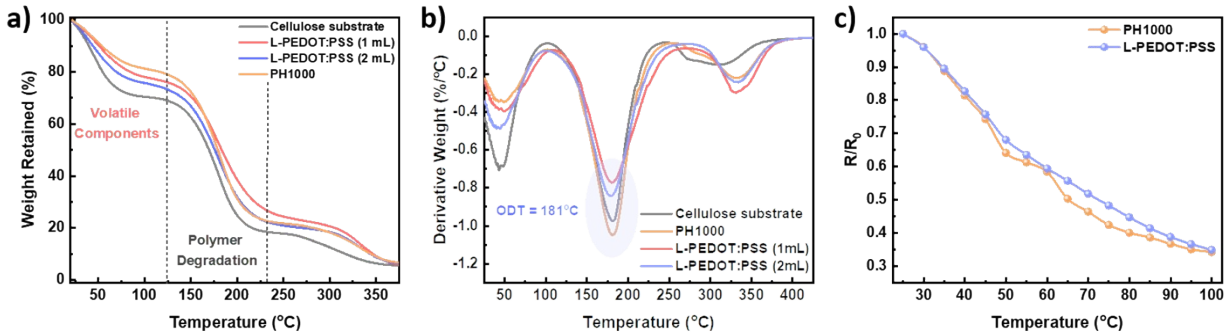

Figure S6. (a-b) Thermogravimetric analysis (TGA) of HEC and HEC/PEDOT:PSS composite films. (c) Variation in relative resistance of HEC/PEDOT:PSS composite films as a function of temperature up to 100°C.

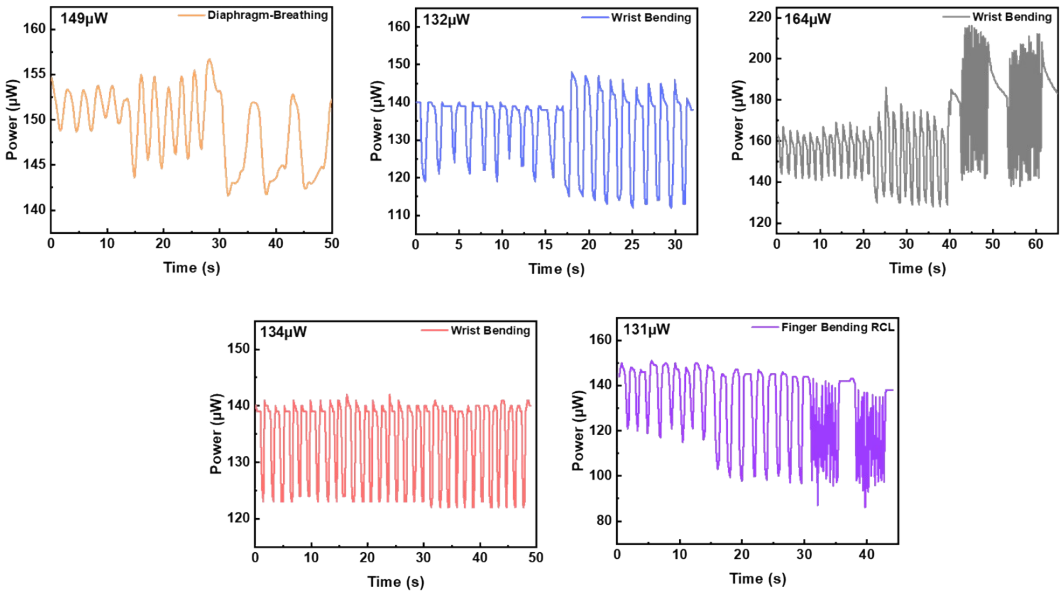

Figure S7. Power consumptions of HEC/PEDOT:PSS composite.

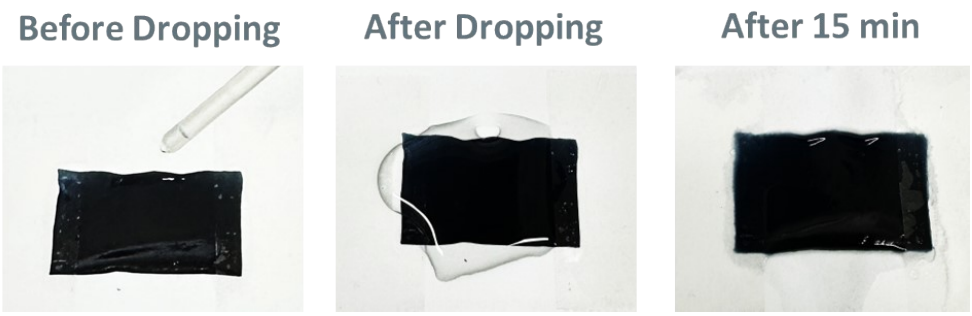

Figure S8. Dropping of water onto the film.

We tested our film by applying approximately 1 mL of water droplets and letting it sit for 15 minutes. The results indicate that 1 mL of water is insufficient to break down the cellulose/L-PEDOT:PSS composite. A small amount of water molecules lacks the energy needed to interact with the high-density cellulose chains through capillary forces and cannot disrupt the hydrogen bonding networks within the cellulose. Because the water content in sweat is insufficient to break the cellulose chains and glycosidic bonds, sweat is expected to evaporate without damaging the cellulose networks.

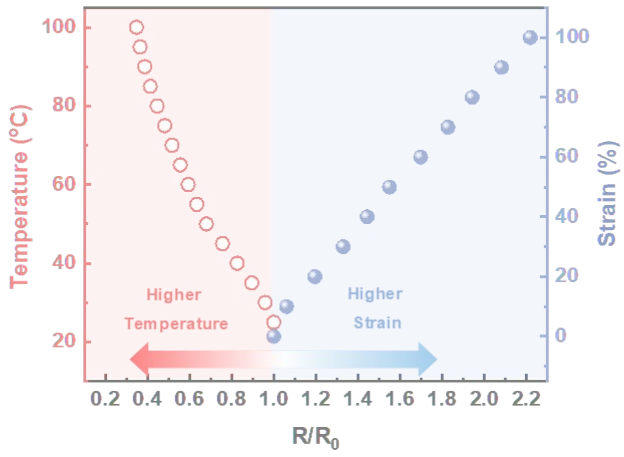

Figure S9. Temperature-resistance-strain plot for HEC/L-PEDOT:PSS composites.

We carried out a simulation to investigate the impact of temperature and strain on the resistance of cellulose/L-PEDOT:PSS composites. In the temperature-dependent region, as the temperature rises from 20°C to 100°C, the normalized resistance (R/R_0) falls below 1, indicating a decrease in resistance with increasing temperature. In the strain-dependent region, the normalized resistance (R/R_0) exceeds 1 as the strain increases from 0% to 100%, indicating that the resistance rises with increasing strain.

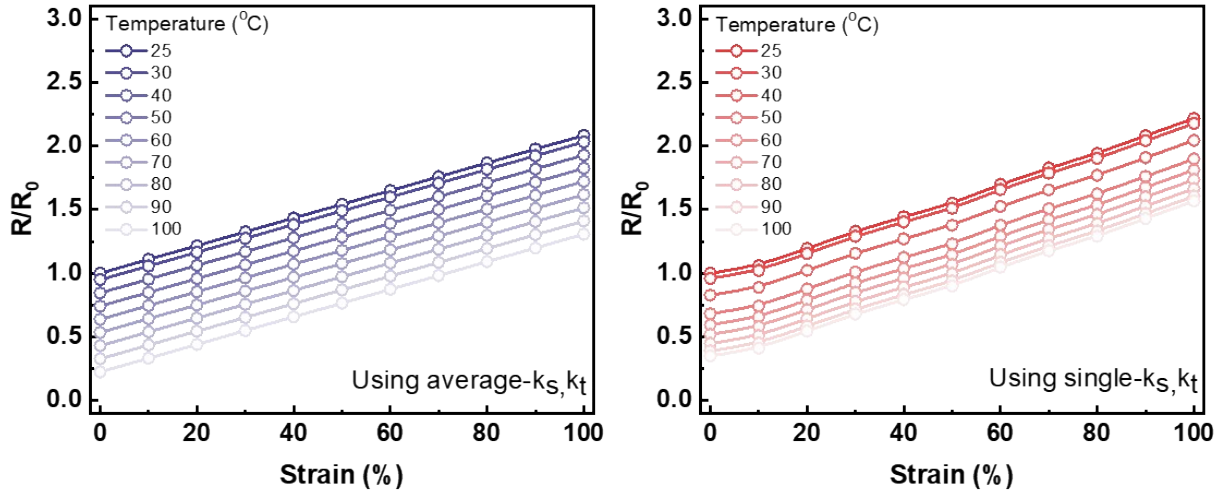

Figure S10. Effect of temperature and strain on the R/R_0 of cellulose/L-PEDOT:PSS composites ($R/R_0 = 1 + k_s \cdot \epsilon + k_t \cdot (T-25)$; k_s: strain sensitivity coefficient, k_t: temperature sensitivity coefficient, ϵ: strain)

We conducted additional simulations to examine the combined effects of mechanical and thermal stimuli on the electrical responses of the sensors. The results show that at a constant temperature, the R/R_0 increases with increasing strain, as indicated by the upward trend of the lines for each temperature. Conversely, at a fixed strain, R/R_0 decreases as the temperature rises. These simulation results are consistent with theoretical predictions and experimental observations, demonstrating that resistance increases with strain and decreases with temperature. Therefore, the simulation effectively illustrate the separate impacts of strain and temperature on the resistance of the cellulose/L-PEDOT:PSS composite sensor.

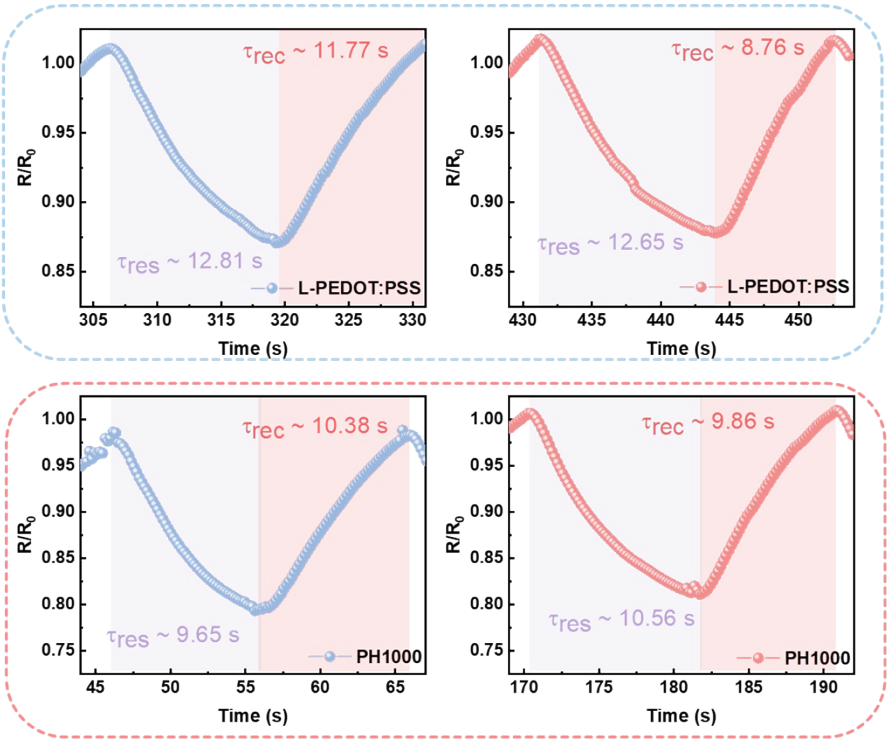

Figure S11. Response and recovery times for temperature sensing.

Our cellulose/L-PEDOT:PSS composite sensors exhibit response times ranging from 9.65 to 12.61 s and recovery times between 8.76 and 11.77 s for temperature sensing. These results highlight their potential reliability for applications requiring rapid and stable temperature measurement. Notably, the response time for strain sensing is faster than that for temperature sensing in cellulose/PEDOT:PSS films. This is because strain sensing involves immediate mechanical deformation, leading to an almost instantaneous change in resistance. In contrast, temperature sensing depends on slower processes such as heat absorption and achieving thermal equilibrium. The inherent response rates of the materials to mechanical versus thermal stimuli also differ, with mechanical adjustments occurring more rapidly. Additionally, heat diffusion introduces a delay in the temperature response. These factors collectively account for the quicker response time observed in strain sensing compared to temperature sensing.

Table S1. Composite films based on cellulose and PEDOT:PSS for flexible and stretchable devices.

Material	Properties	Application	Ref.
CNF/PEDOT:PSS PH1000	Conductivity 100~400 S/cm, non-stretchable	Conducting power papers	[1]
HEC/PEDOT:PSS	Spin-coating method, sheet resistance ~581 Ω/sq, stretchability 60%	Human-skin sensor	[2]
CNF/PEDOT:PSS	Flexible, max. stretchability 9%, tensile stress 106 MPa, conductivity max. 126 S/cm, specific capacitance 854 mF/cm^2	Supercapacitor	[3]
CNF/PEDOT:PSS / MXene	Flexible, Max. stretchability 5%, tensile stress 60 MPa, EMI shielding 76.9 dB, conductivity 1903 S/cm	EMI shielding	[4]
CNF/PEDOT:PSS	Non-stretchable, sheet resistance 5 Ω/sq, capacitances 25 F/g	Capacitor	[5]
PVA/Gly-CNC/PVP/ PEDOT:PSS	Max. stretchability ~500%, self-healable, conductivity ~0.1 S/cm	Human motion detection	[6]

Table S2. PEDOT:PSS-based temperature Sensors.

Active Materials	Properties	TCR	Working Temperature	Ref.
PEN/PEDOT:PSS	Flexible, humidity stability, R_{sh} ~ 75 kΩ, printing method, good stability	-0.77%/°C (25~50°C) ~ -1.14/°C	30 °C ~ 45°C	7
PEN/PEDOT:PSS	Flexible, humidity stability, printing method	-0.25%/°C	20 °C ~ 70°C	8
PDMS/PEDOT:PSS	Microcrack design, pre-stretched 20% and 40%	-0.31%/C (40°C)	25 °C ~ 55°C	9
Textile/PEDOT:PSS	Flexible, R_{sh} ~135 kΩ (length 8 cm) and R_{sh} ~50 kΩ (length 3 cm)	-0.48%/°C	-50°C ~ 80°C	10
PEDOT:PSS/GO	Flexible, printing method	-1.09%/C	25°C ~ 100°C	11
Silk/PEDOT:PSS	Flexible, biodegradable, photolithography method, humidity stability, excellent stability	-0.99%/°C	20°C ~ 50°C	12
Cellulose/L-PEDOT:PSS	Max. strain ε ~ 190% (σ ~ 0.71 MPa), tough, breathable, R_{sh} ~ 78 kΩ/sq, low hysteresis and recyclable	-1.15%/°C (40°C) ~ -1.28%/°C	30°C ~ 100°C	***This Work***

Table S3. Comparison of electromechanical properties between original and recycled films

Cellulose/ PEDOT:PSS	Max. Strain (%)	Max. Stress (MPa)	Toughness (MJ/m^3)	R_{init} (Ω)	$\Delta R/R_0$ (%) (ε=100%)
Original	195	0.711	0.805	78,953	122
Recycled	190	0.9	0.821	100,590	136
Recovery Percentage	**97.4%**	**126.65%**	**101.99%**	**127.4%**	**111.48%**

Table S4. Comparison of sensor performance between original and recycled films

Cellulose/ PEDOT:PSS	$\Delta R/R_0$ ~ Strained Skin	$\Delta R/R_0$ ~ Wrist Bending (90°)	$\Delta R/R_0$ ~ Finger Bending (45°)

Original	15%	25%	17%
Recycled	19%	21%	20%
Recovery Percentage	**126%**	**84%**	**117%**

References

(1) Belaineh, D.; Andreasen, J. W.; Palisaitis, J.; Malti, A.; Håkansson, K.; Wågberg, L.; Crispin, X.; Engquist, I.; Berggren, M. Controlling the Organization of PEDOT:PSS on Cellulose Structures. *ACS Appl. Polym. Mater.* **2019**, *1* (9), 2342–2351. https://doi.org/10.1021/acsapm.9b00444.

(2) Han, J. W.; Wibowo, A. F.; Park, J.; Kim, J. H.; Prameswati, A.; Entifar, S. A. N.; Lee, J.; Kim, S.; Chan Lim, D.; Moon, M. W.; Kim, M. S.; Kim, Y. H. Highly Stretchable, Robust, and Conductive Lab-Synthesized PEDOT:PSS Conductive Polymer/Hydroxyethyl Cellulose Films for on-Skin Health-Monitoring Devices. *Org. Electron.* **2022**, *105* (January), 106499. https://doi.org/10.1016/j.orgel.2022.106499.

(3) Du, H.; Zhang, M.; Liu, K.; Parit, M.; Jiang, Z.; Zhang, X.; Li, B.; Si, C. Conductive PEDOT:PSS/Cellulose Nanofibril Paper Electrodes for Flexible Supercapacitors with Superior Areal Capacitance and Cycling Stability. *Chem. Eng. J.* **2022**, *428* (August 2021), 131994. https://doi.org/10.1016/j.cej.2021.131994.

(4) Liu, K.; Du, H.; Liu, W.; Zhang, M.; Wang, Y.; Liu, H.; Zhang, X.; Xu, T.; Si, C. Strong, Flexible, and Highly Conductive Cellulose Nanofibril/PEDOT:PSS/MXene Nanocomposite Films for Efficient Electromagnetic Interference Shielding. *Nanoscale* **2022**, *14* (40), 14902–14912. https://doi.org/10.1039/d2nr00468b.

(5) Ko, Y.; Kim, J.; Kim, D.; Kwon, G.; Yamauchi, Y.; You, J. Fabrication of Highly Conductive Porous Cellulose/PEDOT: PSS Nanocomposite Paper via Post-Treatment. *Nanomaterials* **2019**, *9* (4). https://doi.org/10.3390/nano9040612.

(6) Lee, Y.; Choi, H.; Zhang, H.; Wu, Y.; Lee, D.; Wong, W. S.; Tang, X. S.; Park, J.; Yu, H.; Tam, K. C. Sensitive, Stretchable, and Sustainable Conductive Cellulose Nanocrystal Composite for Human Motion Detection. *ACS Sustain. Chem. Eng.* **2021**, *9* (51), 17351–17361. https://doi.org/10.1021/acssuschemeng.1c06741.

(7) Wang, Y. F.; Sekine, T.; Takeda, Y.; Yokosawa, K.; Matsui, H.; Kumaki, D.; Shiba, T.; Nishikawa, T.; Tokito, S. Fully Printed PEDOT:PSS-Based Temperature Sensor with High Humidity Stability for Wireless Healthcare Monitoring. *Sci. Rep.* **2020**, *10* (1), 1–8. https://doi.org/10.1038/s41598-020-59432-2.

(8) Bali, C.; Brandlmaier, A.; Ganster, A.; Raab, O.; Zapf, J.; Hübler, A. Fully Inkjet-Printed Flexible Temperature Sensors Based on Carbon and PEDOT: PSS. *Mater. Today Proc.* **2016**, *3* (3), 739–745. https://doi.org/10.1016/j.matpr.2016.02.005.

(9) Yu, Y.; Peng, S.; Blanloeuil, P.; Wu, S.; Wang, C. H. Wearable Temperature Sensors with Enhanced Sensitivity by Engineering Microcrack Morphology in PEDOT:PSS-PDMS Sensors. *ACS Appl. Mater. Interfaces* **2020**, *12* (32), 36578–36588. https://doi.org/10.1021/acsami.0c07649.

(10) Lee, J. W.; Han, D. C.; Shin, H. J.; Yeom, S. H.; Ju, B. K.; Lee, W. PEDOT:PSS-Based Temperature-Detection Thread for Wearable Devices. *Sensors (Switzerland)* **2018**, *18* (9), 2–9. https://doi.org/10.3390/s18092996.

(11) Soni, M.; Bhattacharjee, M.; Ntagios, M.; Dahiya, R. Printed Temperature Sensor Based on PEDOT: PSS-Graphene Oxide Composite. *IEEE Sens. J.* **2020**, *20* (14), 7525–7531. https://doi.org/10.1109/JSEN.2020.2969667.

(12) Pradhan, S.; Yadavalli, V. K. Photolithographically Printed Flexible Silk/PEDOT:PSS Temperature Sensors. *ACS Appl. Electron. Mater.* **2021**, *3* (1), 21–29. https://doi.org/10.1021/acsaelm.0c01017.